

**Figure S1. Two other examples of phospholipid-strip assay. Supplementary information for Figure 1.** **A.** GST-Ct<sub>ASIC1a</sub> fusion proteins were incubated with the membrane strips under different buffering systems: PBS buffer (left, 140 mM NaCl, 3 mM KCl, 10 mM phosphate buffer, 0.1% Tween-20, pH 7.4), or TBS buffer (right, 10 mM Tris, 150 mM NaCl, 0.1% Tween-20, pH 8.0), and then probed with anti-GST antibody. **B.** Detection of purified GST, GST-Nt<sub>ASIC1a</sub>, GST-Ct<sub>ASIC1a</sub>, GST-Nt<sub>ASIC2a</sub>, and GST-Ct<sub>ASIC2a</sub> fusion proteins by Coomassie Blue staining and Western Blotting. **C.** Phospholipid-strip detection of GST proteins fused with the intracellular C-terminal domains of glutamate receptors GluA1, GluA2 and GluN1. **D.** Detection of purified GST, GST-Ct<sub>GluA1</sub>, GST-Ct<sub>GluA2</sub>, GST-Ct<sub>GluN1</sub> fusion proteins by Coomassie Blue staining and Western Blotting. **E.** Diagram illustration of membrane topology and cytosolic domains (orange) of ASIC1a, ASIC2a, GluA1, GluA2 and GluN1.

**Figure S2. Spine enrichment and synaptic location of ASIC1a and Lact-C2. Supplementary information for Figure 2A-2C.**

**A.** Representative confocal images of DIV21-28 rat cortical neurons transfected with EGFP and mCherry-Lact-C2 (left), EGFP and mCherry-ASIC1a (middle), and EGFP and mCherry (right) constructs at DIV7. After fixation, neurons were immunostained with the antibodies of corresponding fluorescent proteins. Examples for neuronal dendrites (blue rectangle) are also shown in high-magnification images. **B.** Representative confocal images of DIV21-28 cortical neurons transfected with EGFP and mCherry-Lact-C2-AAA at DIV7. Examples for neuronal dendrites (blue rectangle) are also shown in high-magnification images. **C.** Comparison of the distributions between wild type Lact-C2 and Lact-C2-AAA in cortical neurons. Signal variability of each group is indicated by coefficient of variation (C.V.).  $n = 10$  cells.  $***p < 0.001$  (unpaired Student's *t*-test). **D.** Comparison of the distributions between Lact-C2 and Lact-C2-AAA in different compartments of DIV21-28 rat cortical neurons.  $n = 10$  cells.  $**p = 0.0075$ ,  $***p < 0.001$  (unpaired Student's *t*-test). **E.** Representative confocal images of DIV28 rat cortical neurons transfected with EGFP at DIV7. After fixation, the neurons were immunostained with the antibodies of PSD-95 (left) or

Synapsin I (right).

**Figure S3. Super-resolution images showing synaptic localization of ASIC1a and Lact-C2. Supplementary information for Figure 2.**

**A.** Representative SIM z-stack maximum projection images of one dendrite of DIV28 rat cortical neuron transfected with EGFP-ASIC1a and mCherry-Lact-C2 on DIV7, imaged with structured illumination microscopy (SIM). After fixation, neurons were immunostained with the antibodies of PSD-95 and corresponding fluorescent proteins. Red arrowheads indicate PSD areas. Spines marked with numbers (in the lower panel) are shown sequentially in (B). **B.** Six examples of spines in the same dendrite shown in (A). Arrowheads, PSD areas; white lines, line scan areas in (C). **C.** Intensity profiling of line scan areas through the spine heads from (B). ASIC1a, green lines; Lact-C2, red lines; PSD-95, blue lines. **D.** 3D reconstruction of the six example spines in (B). Arrowheads, PSD areas. **E.** Correlation plots of the areas of spine ASIC1a (green,  $R^2 = 0.7547$ , slope =  $0.5066 \pm 0.0222$ ,  $p < 0.0001$ , Spearman's test) or Lact-C2 (red,  $R^2 = 0.7781$ , slope =  $0.5674 \pm 0.0232$ ,  $p < 0.0001$ , Spearman's test) vs. spine head areas,  $n = 172$  spines from 7 cells. **F.** Correlation plots of the areas of spine ASIC1a (green,  $R^2 = 0.5226$ , slope =  $1.335 \pm 0.0979$ ,  $p < 0.0001$ , Spearman's test) or Lact-C2 (red,  $R^2 = 0.4753$ , slope =  $1.405 \pm 0.1132$ ,  $p < 0.0001$ , Spearman's test) vs. PSD areas,  $n = 172$  spines from 7 cells. **G.** Correlation plots of PSD areas vs. spine head areas ( $R^2 = 0.4850$ , slope =  $0.2199 \pm 0.0174$ ,  $p < 0.0001$ , Spearman's test),  $n = 172$  spines from 7 cells. **H.** Representative SIM z-stack maximum projection image (left) and 3D reconstruction (right) of one dendrite of DIV28 *Asic1a*<sup>-/-</sup> mouse cortical neuron transfected with HA-ASIC1a on DIV7. Neurons were stained with anti-HA antibody under non-permeabilized conditions for surface ASIC1a and with anti-PSD-95 antibody under permeabilized conditions for PSD-95. **I.** Cumulative probabilities of densities of surface ASIC1a nanoclusters distributed in different compartments of cortical neurons. **J & K.** Frequency distributions of the numbers of surface ASIC1a nanoclusters in spine head (J) or spine neck (K). **L.** Frequency distribution of the diameters (semi-major axis) of surface ASIC1a nanoclusters.

#### **Figure S4. Postsynaptic localizations of GluN1.**

**A.** Representative super-resolution images of a DIV28 rat cortical neuron transfected with EGFP-GluN1 and mCherry on DIV7, imaged with SIM. After fixation, neurons were immunostained with the antibodies of PSD-95 and corresponding fluorescent protein. More details about the spines marked with numbers are shown individually in (B) and (C). **B.** SIM z stack maximum projection images of dendritic spines marked in (A). White lines, line scan areas through the spine heads, with the intensity profiling shown at right. Green lines, GluN1; red dash lines, mCherry; blue lines, PSD-95. **C.** 3D reconstruction images of the spine heads shown in (B). **D.** Colocalization analysis between GluN1 and PSD-95 (or mCherry). Bars indicate mean  $\pm$  SEM,  $n = 50$  spines from 10 cells.  $***p < 0.001$  (Student's *t*-test). **E.** Schematic diagram of four patterns of synaptic localizations of GluN1 and PSD-95. Green, GluN1; blue, PSD-95; cyan, colocalization area.

#### **Figure S5. Comparison of confocal and Airyscan imaging results.**

**A.** Representative confocal image and super-resolution image (Airyscan) of the same DIV28 neuron transfected with EGFP-ASIC1a and mCherry-Lact-C2 on DIV7. After fixation, neurons were immunostained with the antibodies of PSD-95 and corresponding fluorescent proteins. **B.** Comparison between confocal and Airyscan images of the same neuronal dendrite. Scale bar = 5  $\mu\text{m}$ . **C-E.** Colocalization analysis between ASIC1a and Lact-C2 (C), Lact-C2 and PSD-95 (D), ASIC1a and PSD-95 (E). Bars indicate mean  $\pm$  SEM,  $n = 9$  cells.  $*p = 0.0242$ ,  $***p = 0.0004$  (Student's *t*-test).

#### **Figure S6. Surface distribution of ASIC1a in cortical neurons.**

**A & B.** Representative confocal images of DIV28 cultured rat cortical neurons transfected with HA-ASIC1a on DIV7. After fixation, neurons were immunostained before permeabilization with monoclonal HA antibody followed by Alexa-488-labeled secondary antibody (1<sup>st</sup> panel from left) to visualize surface ASIC1a and after permeabilization with monoclonal HA antibody (A) or polyclonal HA antibody (B)

followed by corresponding Alexa-568-labeled secondary antibody (2<sup>nd</sup> panel) to label total or cytoplasmic ASIC1a, respectively. 3<sup>rd</sup> panel, merged image for 1<sup>st</sup> and 2<sup>nd</sup> panels; 4<sup>th</sup> panel, another example in the same experiment. C, cytoplasmic ASIC1a; S, surface ASIC1a; T, total ASIC1a. **C.** High-magnification images of neuronal dendrites in boxed areas of (A) and (B). **D.** Surface fraction of ASIC1a (surface/total ratio) during neurodevelopment *in vitro* (2-5 weeks). n = 5.  $p = 0.0007$ , vs. DIV14 group (one-way ANOVA with Tukey's post hoc); \* $p < 0.05$ , \*\* $p < 0.01$ , \*\*\* $p < 0.001$ .

**Figure S7. Juxtamembranous location of PS-binding motif.**

**A.** Sequences and structures of TMII and proximal C-terminus of ASIC1a. **A1**, Alignment of juxtamembranous domains of ASIC1a C-terminus. TMII domains resolved by different chicken ASIC1 crystal structures are printed in blue. Unresolved flexible regions are shown in gray. Arginines in the di-arginine motif are printed in red. Note that the resolved TMII helices are of different lengths. **A2**, bottom view of the intracellular stretches and the transmembrane domain of ASIC1a channel (PDB 6AVE). The two transmembrane regions, TMI and TMII, of one subunit and the short stretches of N- and C-termini are shown in blue and yellow, respectively. **A3**, side view of the transmembrane and proximal cytoplasmic domains of superimposed closed and open states of ASIC1a channels. The resting state from PDB 6AVE is shown in gray, while the open state from PDB 4NTW is shown in orange. Note that TMII is separated in two parts, TM2a and TM2b, by a GAS belt (labeled in pink in A1). **B.** ASIC1a TMII domain sequences predicted by hydrophobicity analysis using computer algorithms listed at left. **C.** Alignment of the second transmembrane helices and proximal C-terminal domains of ASIC and ENaC family members.

**Figure S8. Surface ASIC1a and PS are both highly enriched and colocalized at the leading edge of CHO cells.**

**A.** Two more examples for Figure 5D. Representative confocal images of CHO cells transfected with N-terminal EGFP-tagged HA-ASIC1a and mCherry-Lact-C2. After fixation, cells were immunostained with anti-HA under non-permeabilized conditions



to visualize surface ASIC1a (sASIC1a or s), followed by staining with anti-EGFP under permeabilized conditions to visualize total ASIC1a (tASIC1a or t) and with anti-mCherry for Lact-C2. Arrowheads indicate leading edges of the cells. White lines indicate line scan areas in (B). **B.** Intensity profiling of line scan areas through the leading edge from (A, last panel).

**Figure S9. Uncoupling PS-ASIC1a interaction alters synaptic targeting of ASIC1a.**

**A & B.** Cumulative probabilities of Pearson's correlation coefficients between total ASIC1a and Lact-C2 (A), or PSD-95 (B).  $n = 200$  spines from 10 cells. **A.**  $**p = 0.048$ , one-way ANOVA with Turkey's post hoc. WT vs  $^{467}\text{EE}^{468}$ , n.s.;  $^{467}\text{EE}^{468}$  vs  $^{467}\text{KK}^{468}$ ,  $**p < 0.01$ ; WT vs  $^{467}\text{KK}^{468}$ , n.s. **B.**  $**p = 0.009$ , one-way ANOVA with Turkey's post hoc. WT vs  $^{467}\text{EE}^{468}$ ,  $**p < 0.01$ ;  $^{467}\text{EE}^{468}$  vs  $^{467}\text{KK}^{468}$ , n.s.; WT vs  $^{467}\text{KK}^{468}$ , n.s. **C & D.** Frequency distributions (C) and cumulative probabilities (D) of Pearson's correlation coefficients between Lact-C2 and PSD-95 for each group.  $n = 200$  spines from 10 cells.  $p = 0.2417$ , one-way ANOVA with Turkey's post hoc. WT vs  $^{467}\text{EE}^{468}$ , n.s.;  $^{467}\text{EE}^{468}$  vs  $^{467}\text{KK}^{468}$ , n.s.; WT vs  $^{467}\text{KK}^{468}$ , n.s.



Figure S1

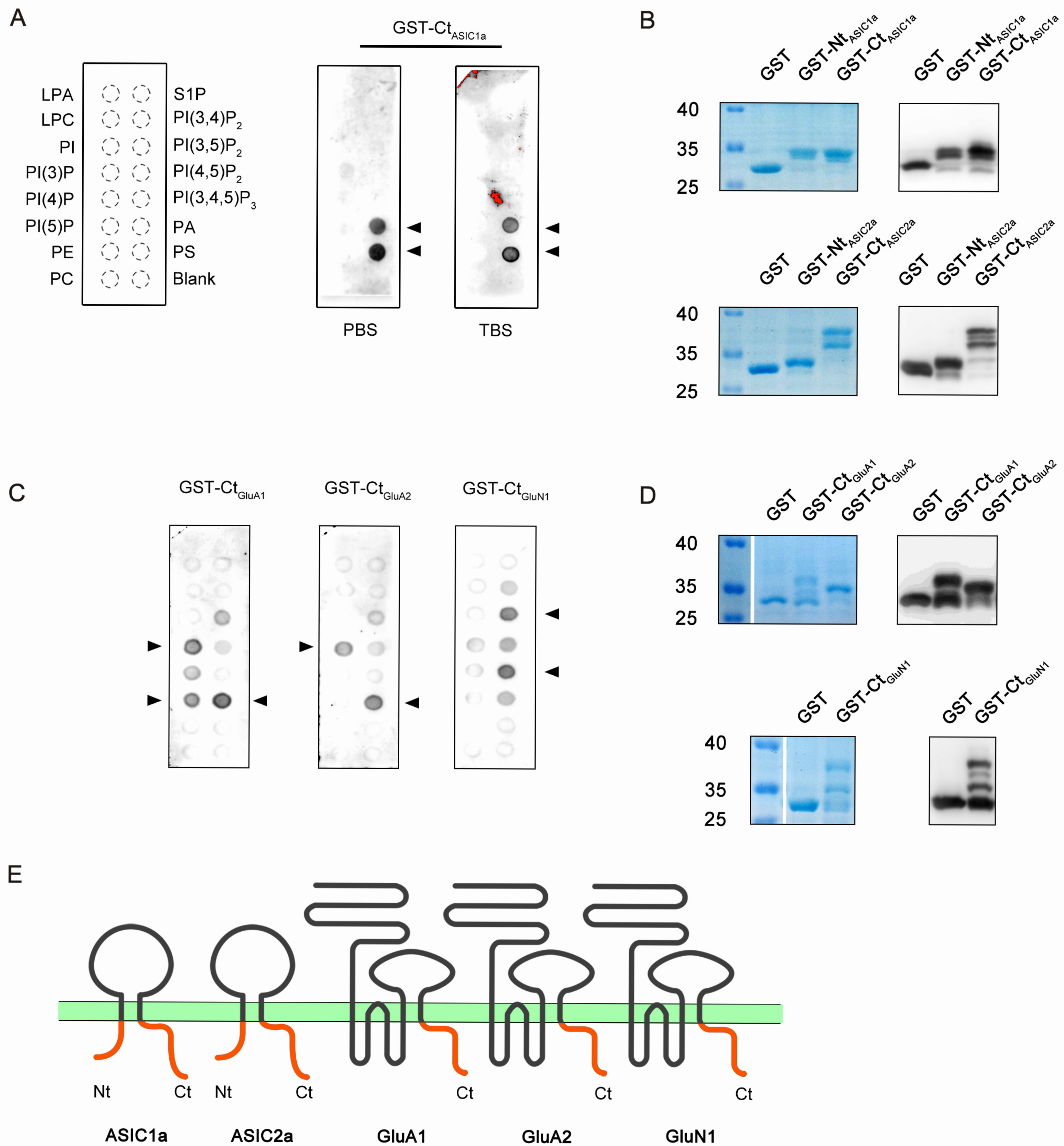




Figure S2

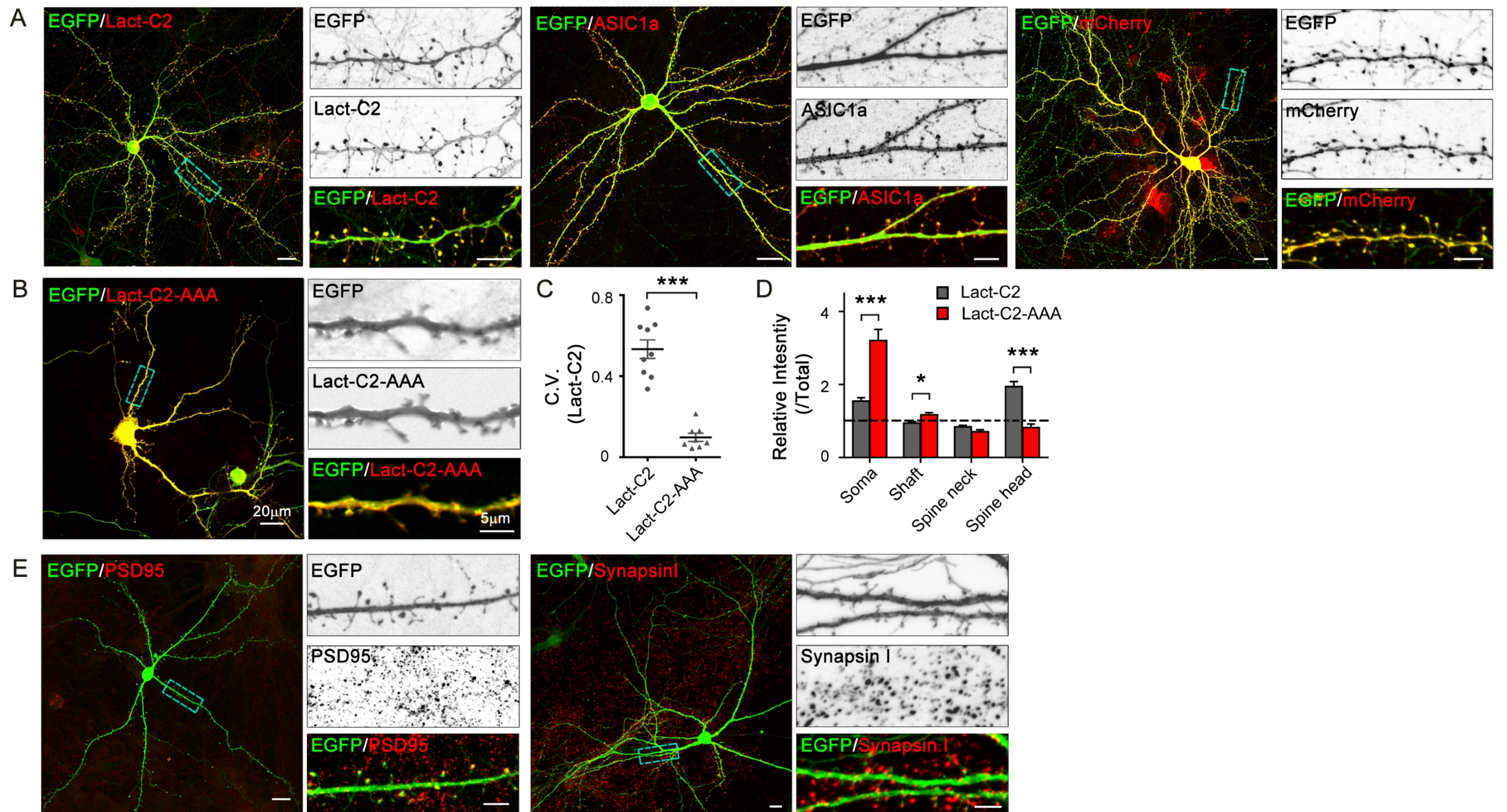




Figure S3

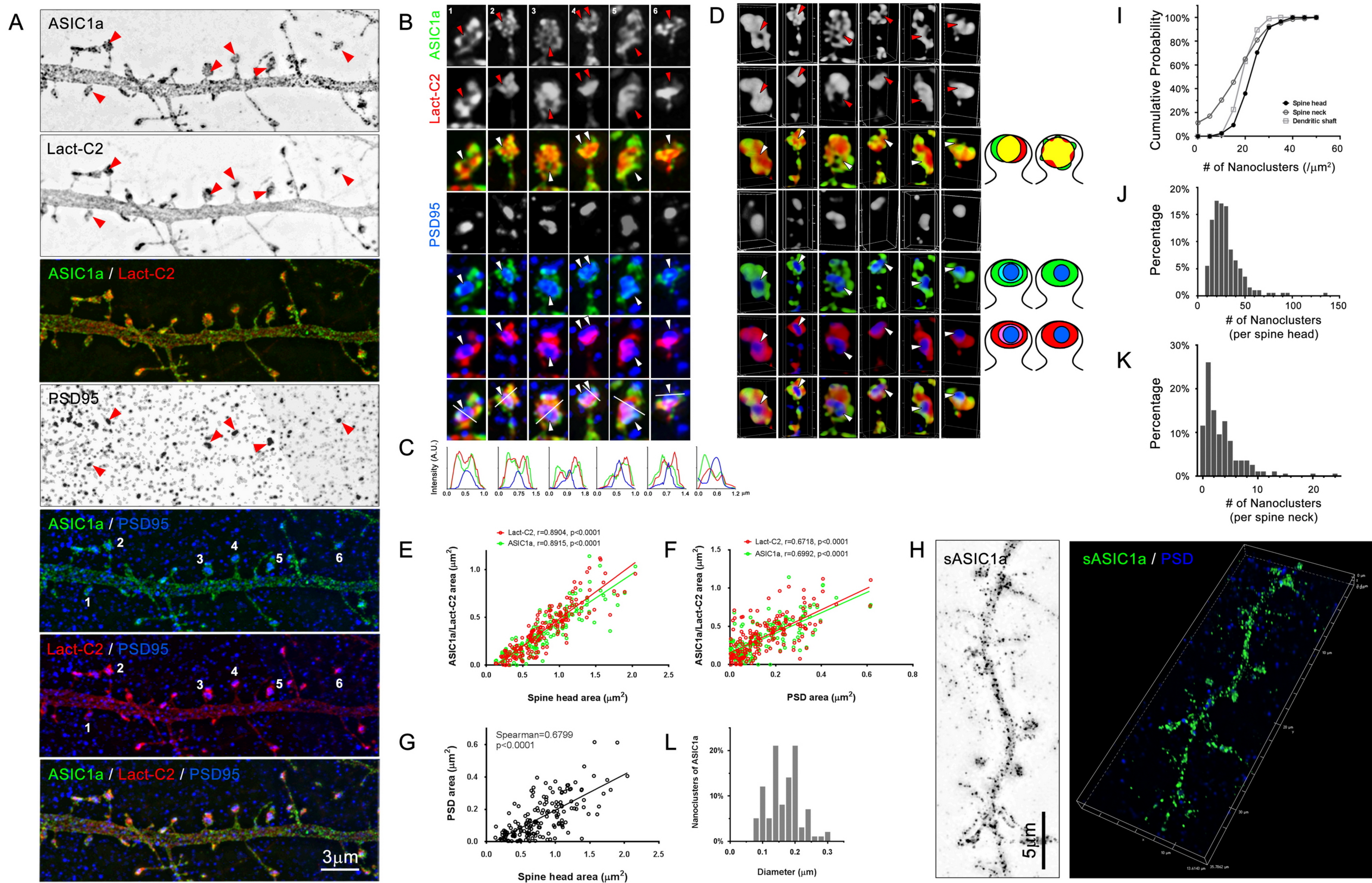




Figure S4

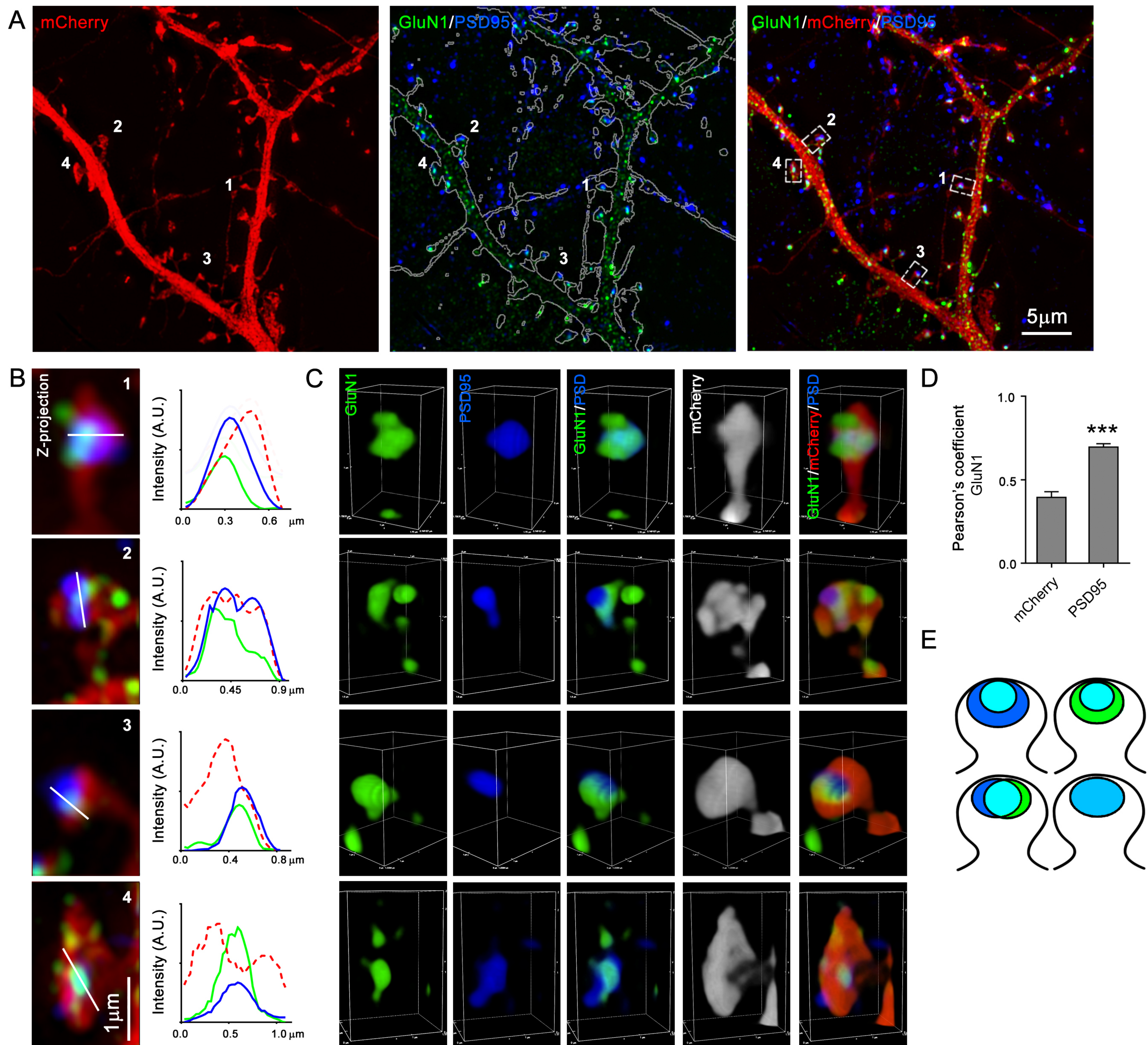




Figure S5

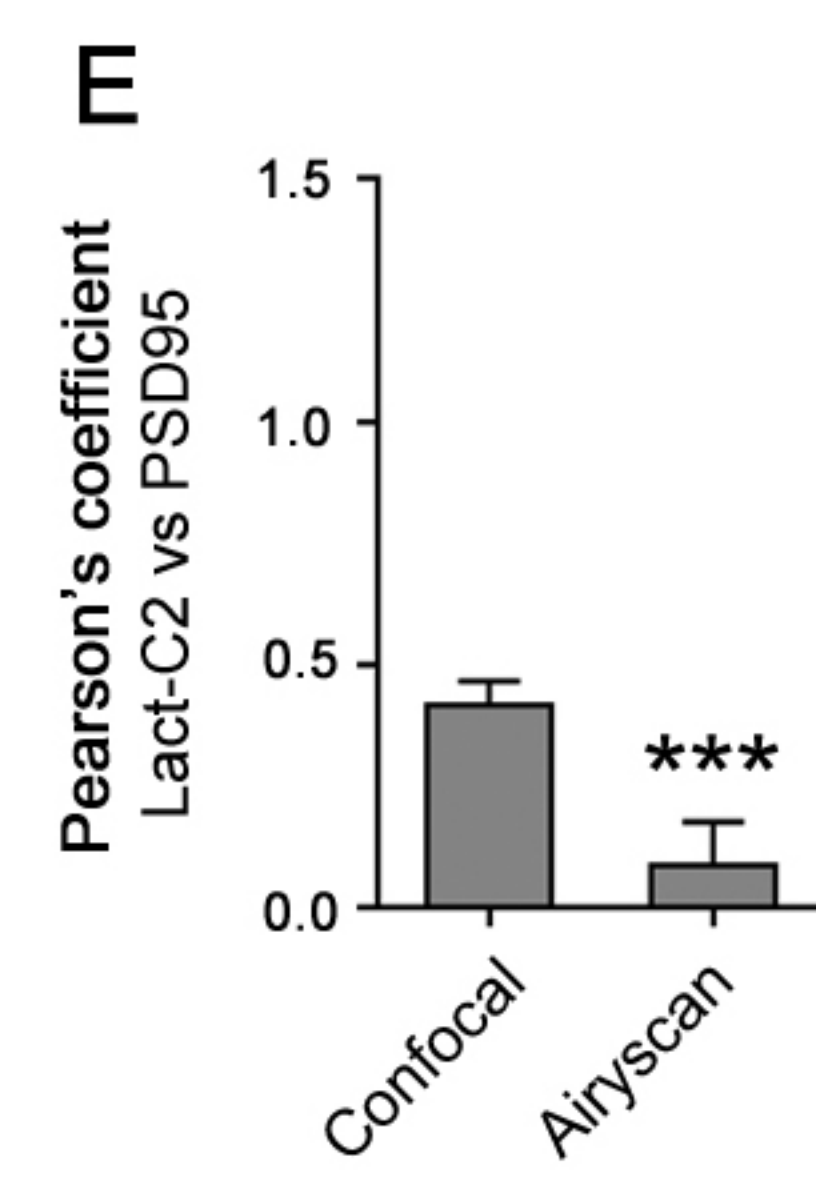
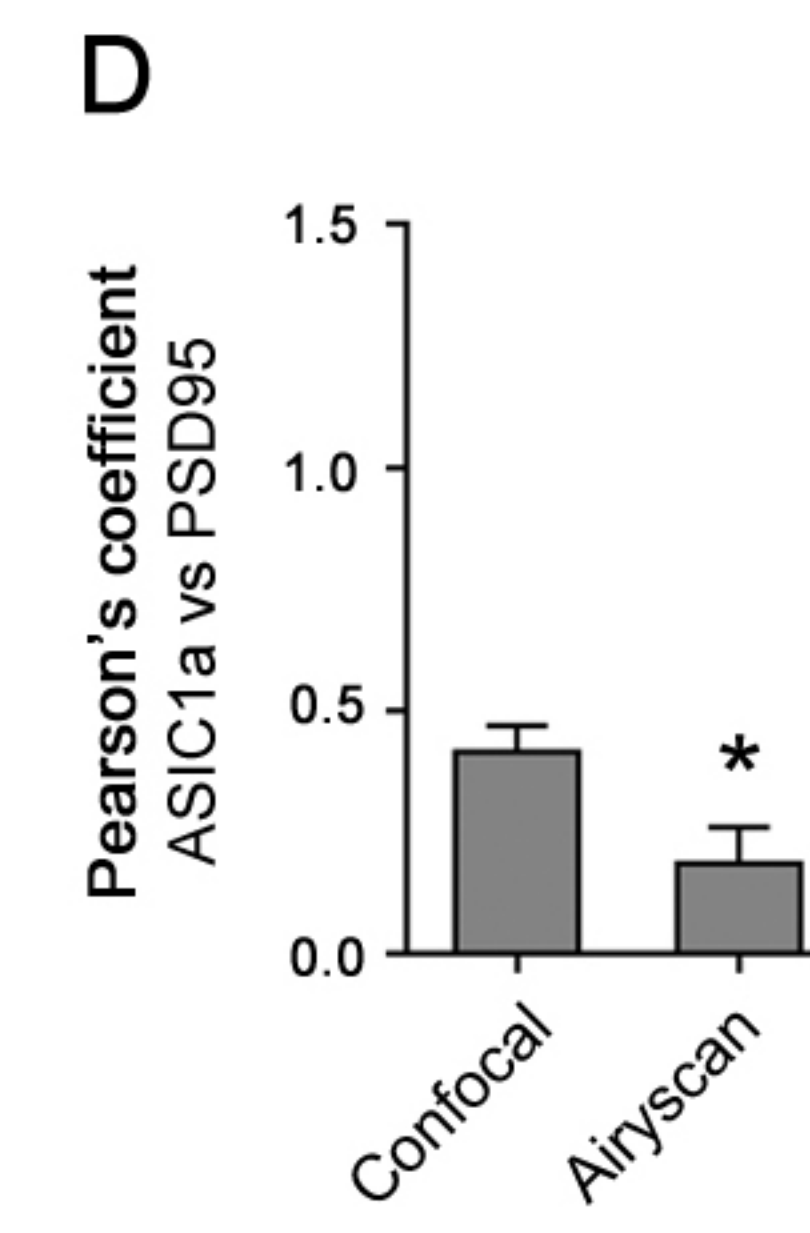
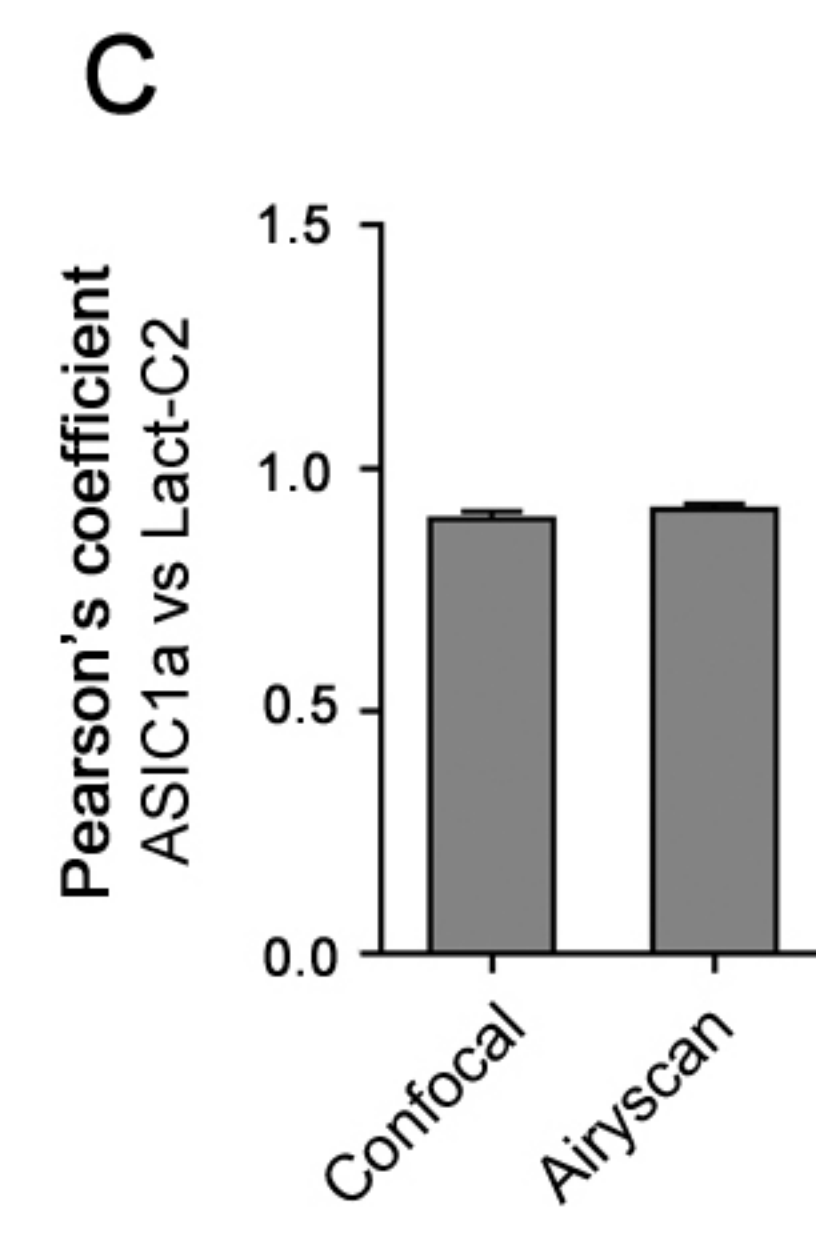
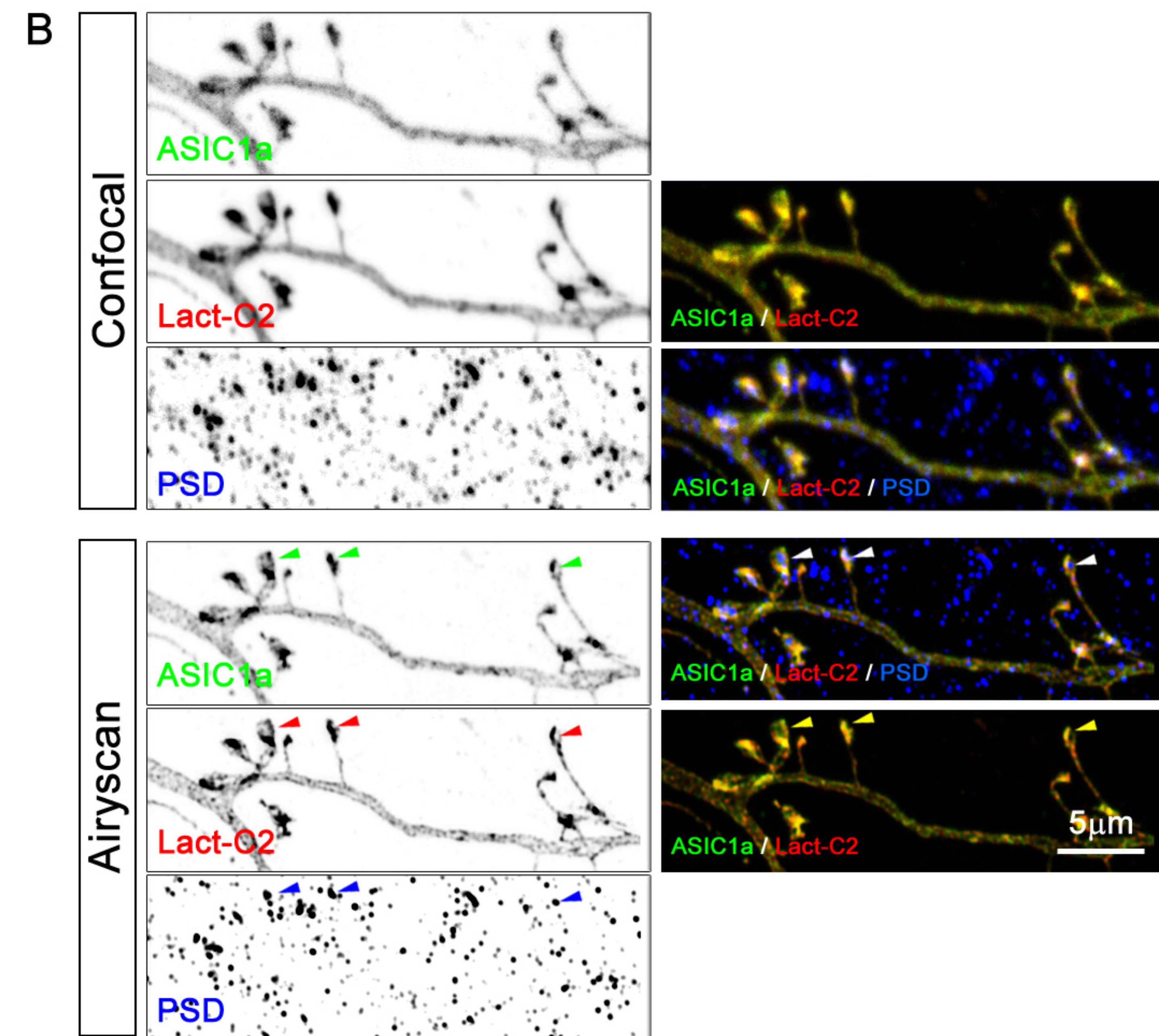
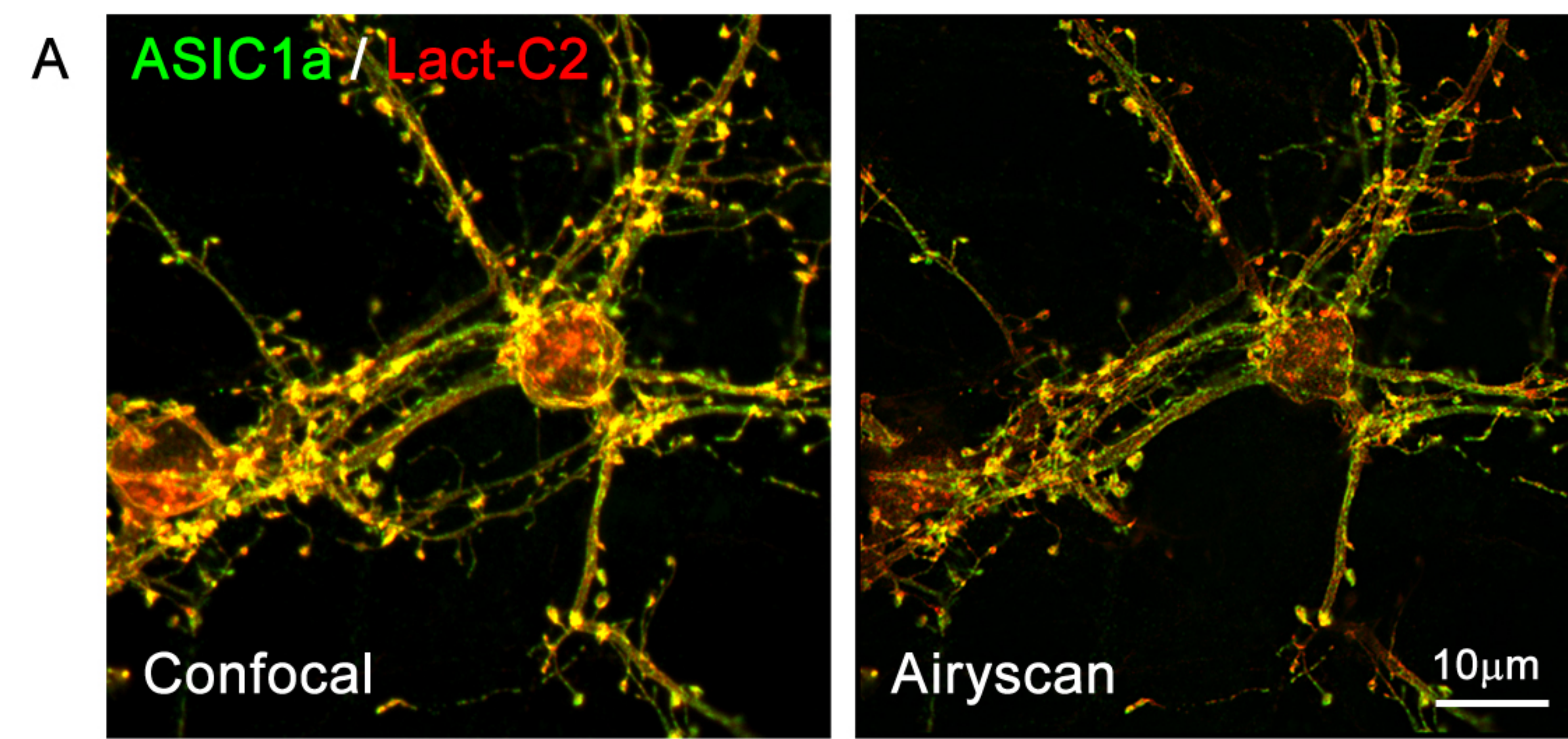




Figure S6

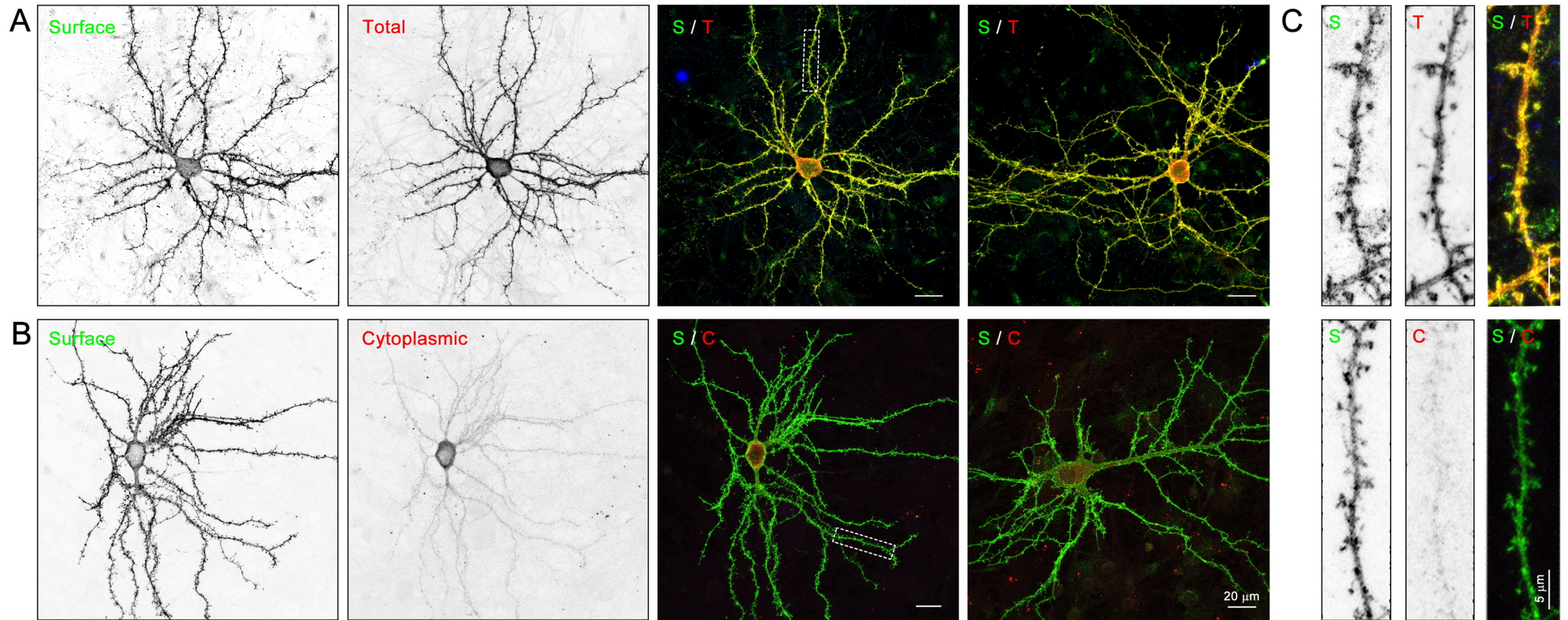
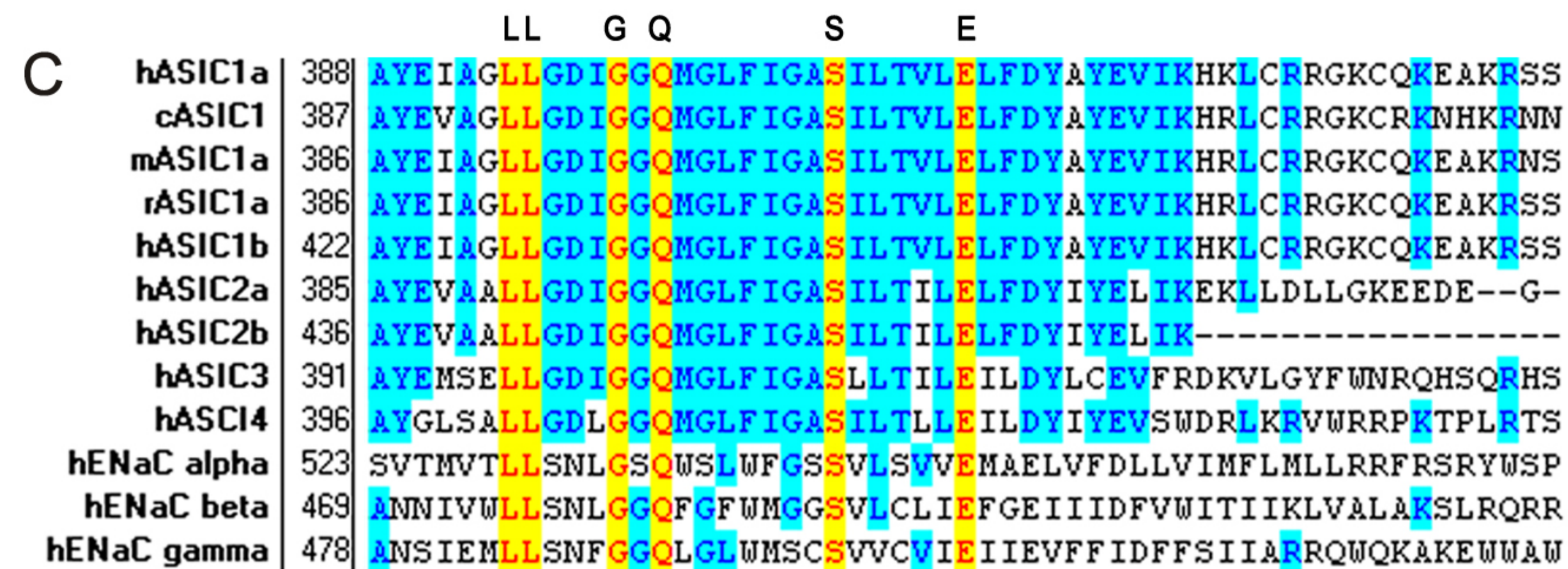
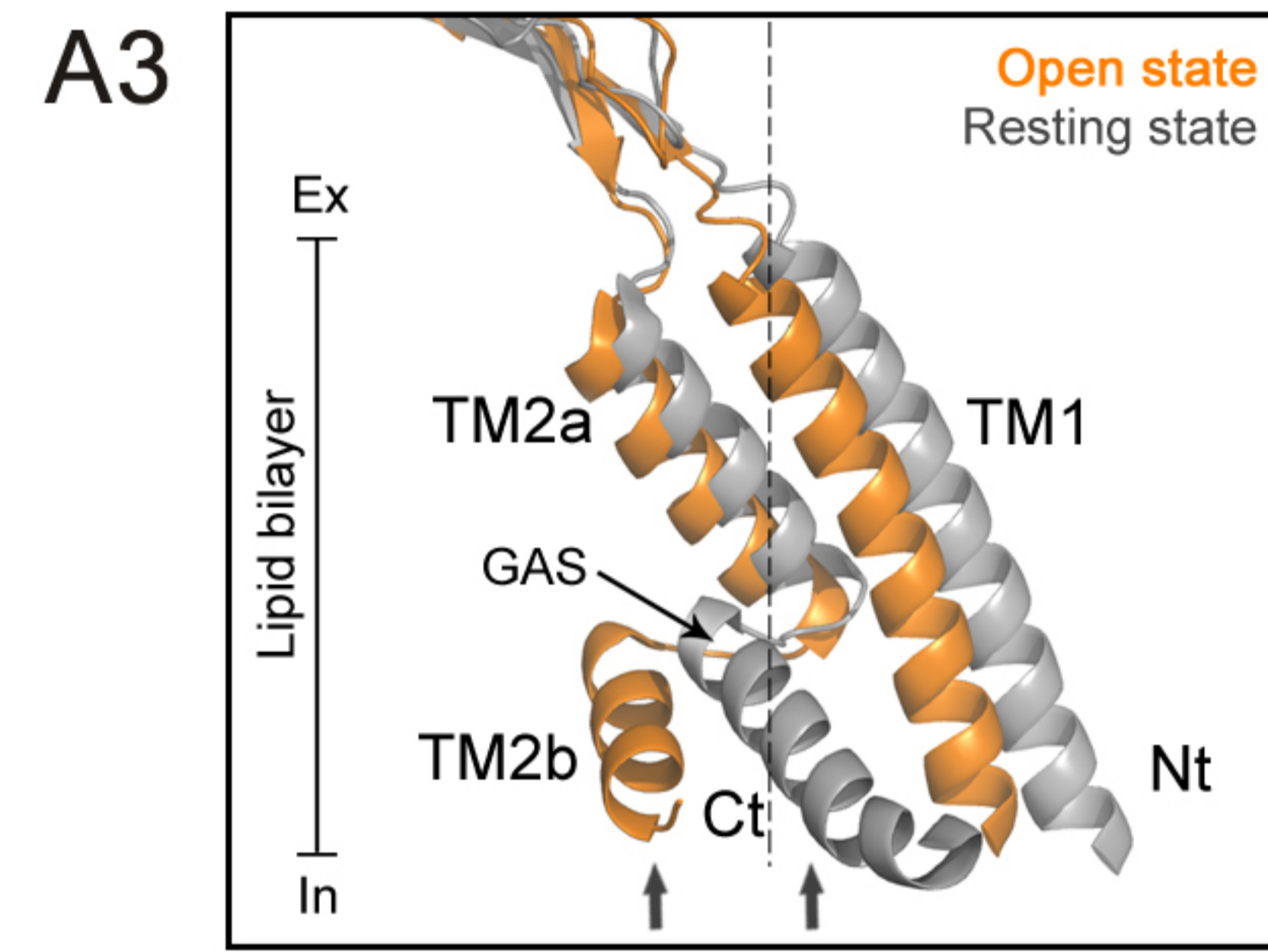
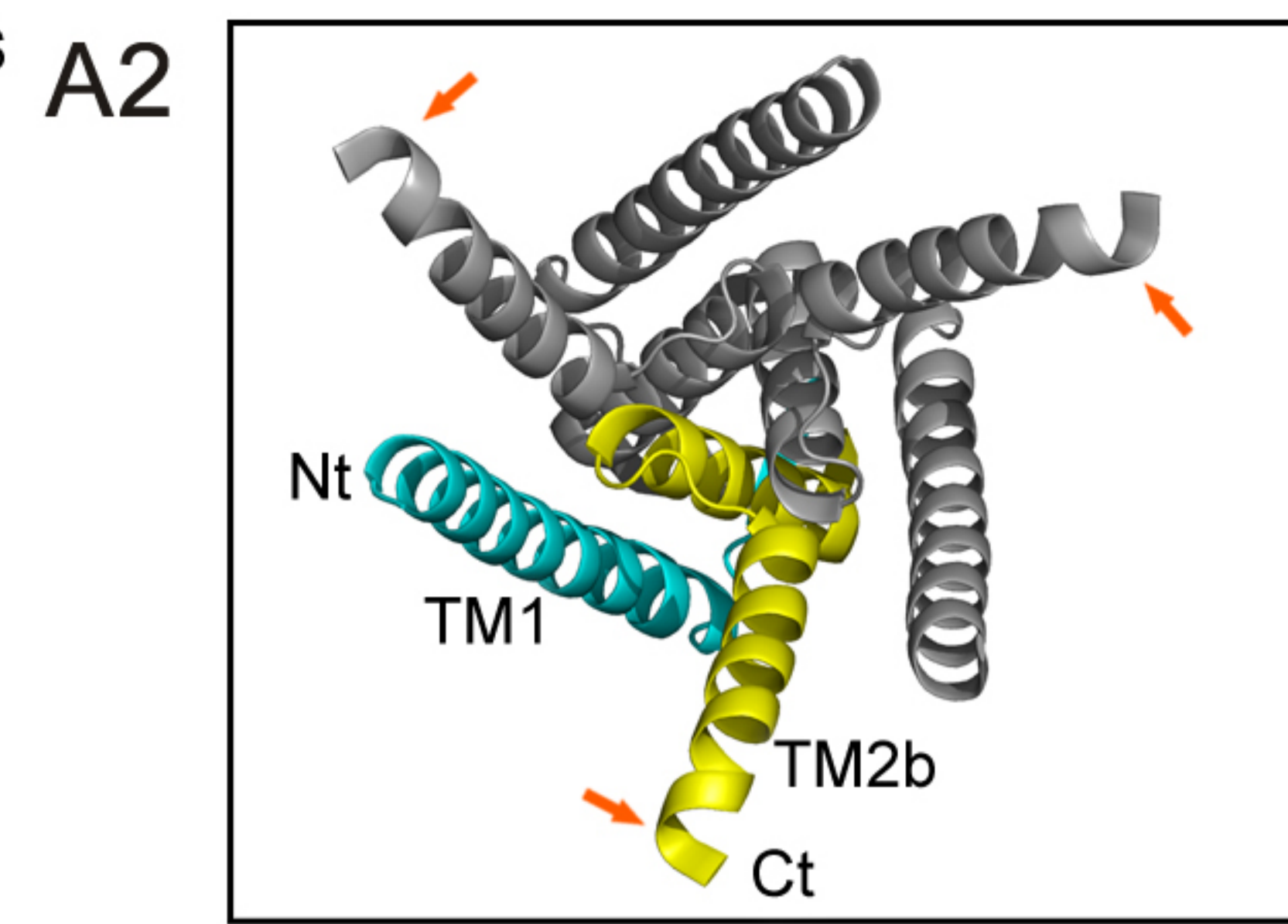
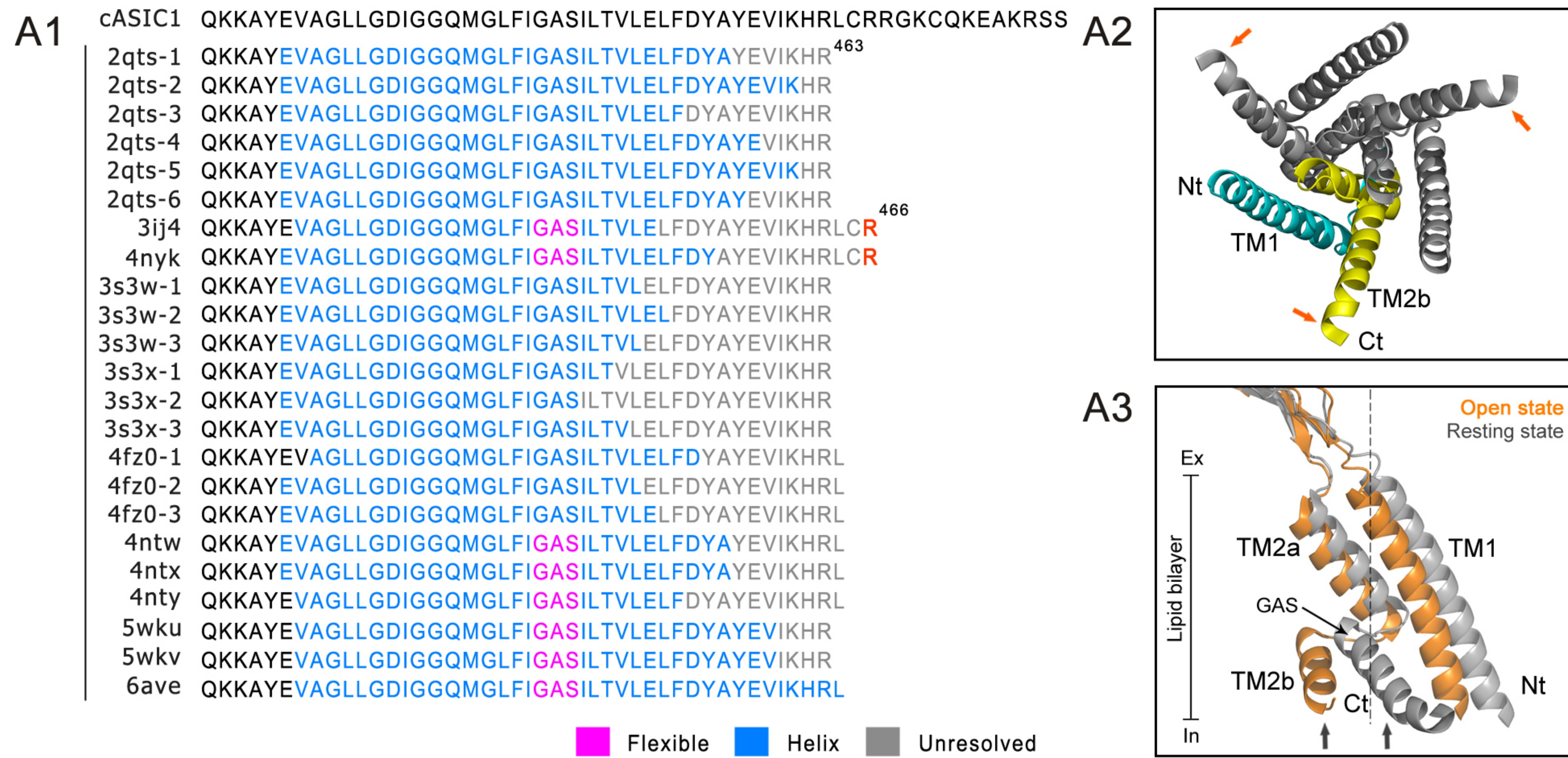




Figure S7





**Figure S8**

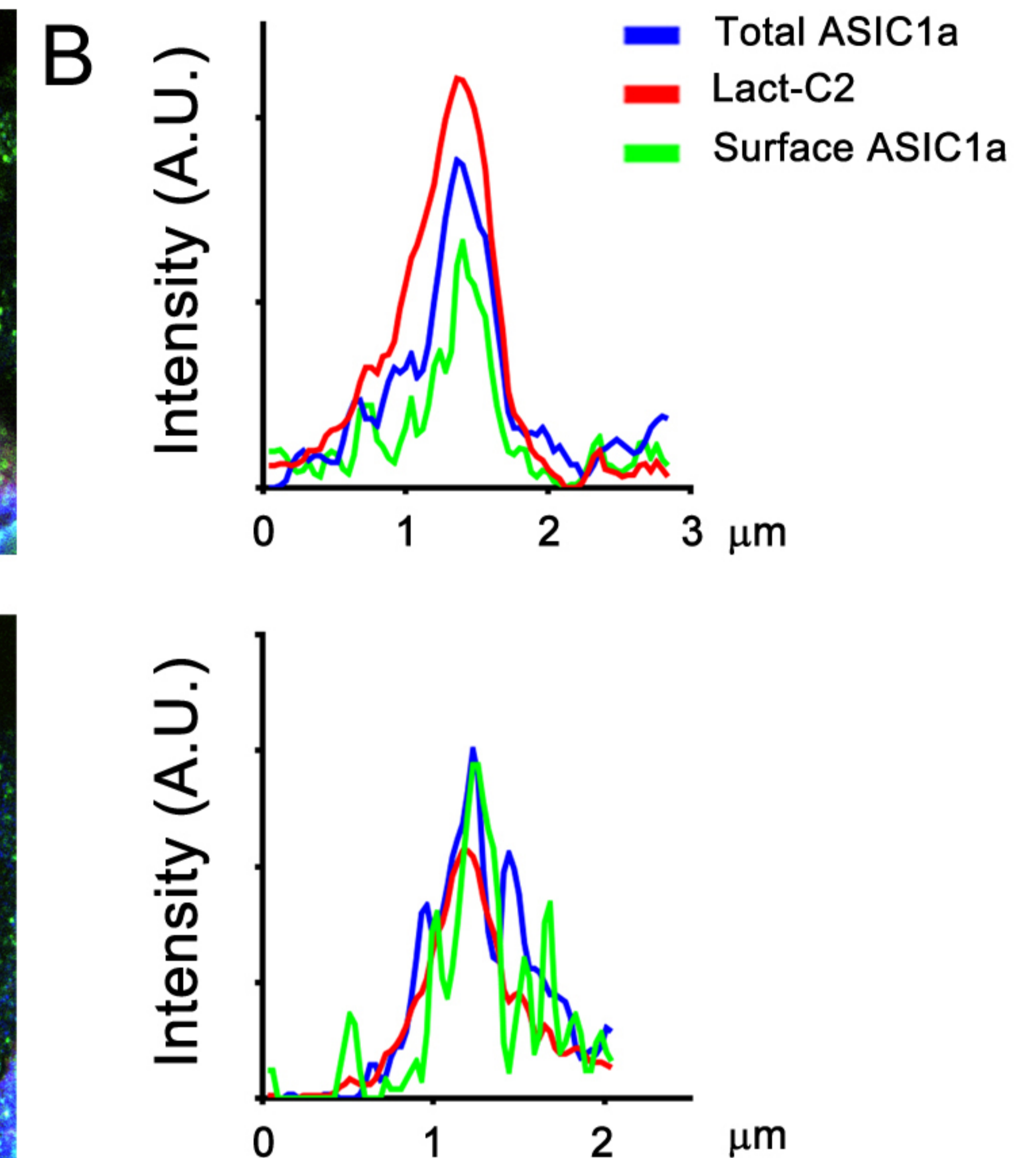
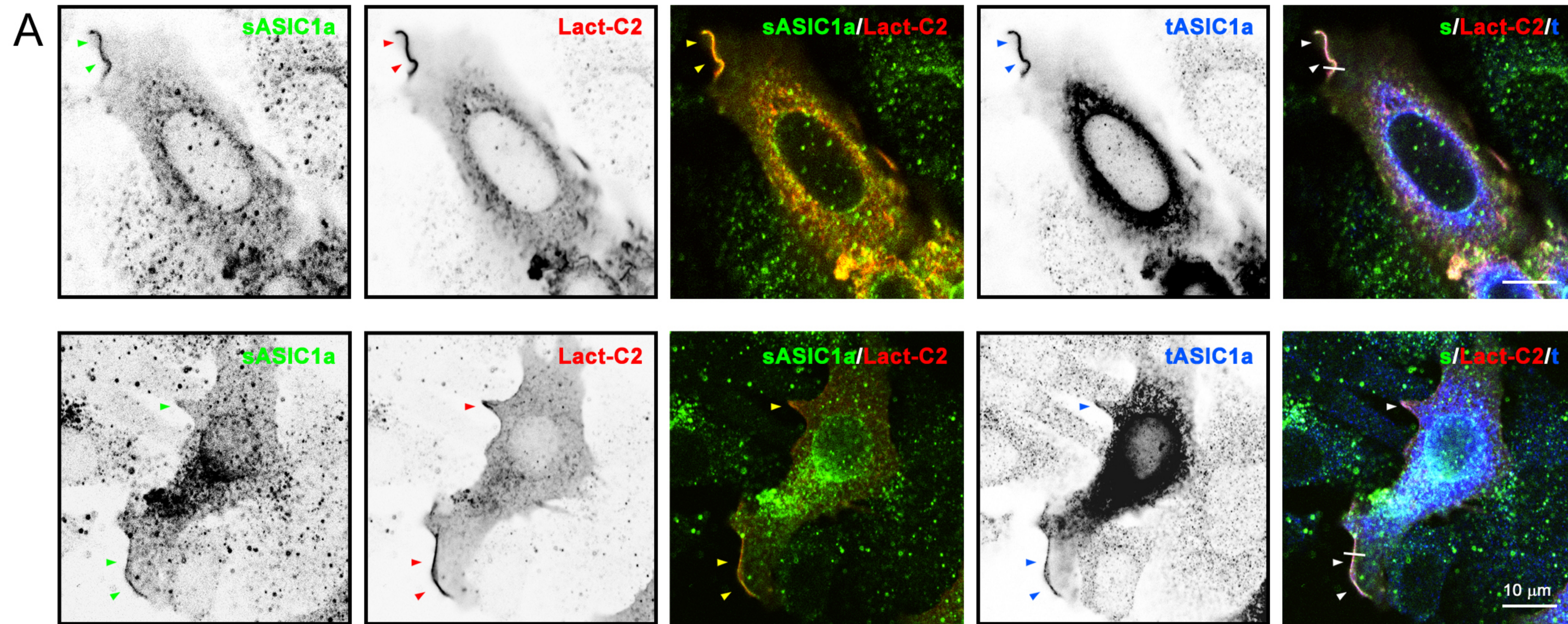




Figure S9

